fractal and fractional

MDPI

Article

Actor-Critic Neural-Network-Based Fractional-Order Sliding Mode Control for Attitude Tracking of Spacecraft with Uncertainties and Actuator Faults

Chenghu Jing *, Xiaole Ma, Kun Zhang, Yanfeng Wang, Bingsheng Yan and Yanbo Hui

School of Mechanical and Electronic Engineering, Henan University of Technology, Zhengzhou 450001, China; ma19513316208@outlook.com (X.M.); kungzhang@haut.edu.cn (K.Z.); yanfengwang@haut.edu.cn (Y.W.); yanbingsheng@haut.edu.cn (B.Y.); yanbohui@hotmail.com (Y.H.)
* Correspondence: chhjing@haut.edu.cn

Abstract: This paper investigates the attitude control of rigid spacecraft in the presence of uncertainties, disturbances, and actuator faults. In order to effectively address these challenges and improve the performance of the system, a novel actor-critic neural-network-based fractional-order sliding mode control (ACNNFOSMC) has been developed for spacecraft. The integration of actor-critic neural network, fractional-order theory, and sliding mode control enables dual functionality: the actor-critic neural network serves to approximate the aggregate of uncertain parameters, disturbances, and actuator faults, thereby facilitating their compensation, while the fractional-order sliding mode control mechanism significantly improves the system's tracking precision and overall robustness against uncertainties. Theoretical analyses are presented to analyze the stability of the proposed control framework. Thorough examination via simulation experiments affirms the effectiveness and control precision of attitude of our proposed control strategy, even in complex operational scenarios.

Keywords: spacecraft; attitude tracking; neural network; sliding mode control; fractional-order

check for updates

Citation: Jing, C.; Ma, X.; Zhang, K.; Wang, Y.; Yan, B.; Hui, Y. Actor-Critic Neural-Network-Based Fractional-Order Sliding Mode Control for Attitude Tracking of Spacecraft with Uncertainties and Actuator Faults. *Fractal Fract.* **2024**, *8*, 385. https://doi.org/10.3390/fractalfract8070385

Academic Editor: António Lopes

Received: 1 June 2024
Revised: 25 June 2024
Accepted: 26 June 2024
Published: 28 June 2024

Copyright: © 2024 by the authors. Licensee MDPI, Basel, Switzerland. This article is an open access article distributed under the terms and conditions of the Creative Commons Attribution (CC BY) license (https://creativecommons.org/licenses/by/4.0/).

1. Introduction

In the pursuit of advanced space missions, spacecraft systems serve as crucial components, requiring exceptional performance attributes like high-precision tracking, robustness, rapid responsiveness, and operational efficiency, all while enduring diverse and challenging environmental conditions [1–3]. It is a widely accepted fact that spacecraft confront inherent uncertainties and experience extrinsic disturbances, compounded by potential actuator malfunctions, which pose significant hurdles to optimal control [4]. Considering the intricacies involved, the attitude control of spacecraft has emerged as a critical research focus due to its centrality in ensuring accurate navigation and maneuverability [5].

Over the past years, concerted efforts have been dedicated to the development of sophisticated attitude tracking control methodologies, such as RISE control [6], adaptive control [7], backstepping control [8], iterative learning control [9], robust H∞ control [10] and so on. Nonetheless, these approaches fundamentally guarantee either asymptotic error convergence or uniform ultimate bounding of the attitude tracking error. In response, finite-time controllers have been vigorously explored [11–16], underscoring the quest for enhanced performance in practical scenarios. Among these methods, terminal sliding mode control has emerged as a potent tool, representing an advancement over conventional sliding mode control (SMC) [17]. It boasts robust characteristics and enables finite-time convergence, albeit its implementation is hampered by issues of singularity and chattering [18,19]. Pukdeboon designed a second-order SMC approach for the attitude control of spacecraft [20], while Lu and Xia introduced an adaptive super-twisting algorithm addressing the uncertainties and external disturbances in spacecraft attitude control [21]. High-order sliding mode effectively overcomes the chattering of classical sliding mode control, and has good robustness and fast response.

The integration of fractional-order calculus with sliding mode control methodologies has provided new means to advance controller performance [22]. By transcending traditional integer-order derivatives, fractional-order differentiation transforms the control signal's sharp transitions into smoother fractional derivatives, effectively suppressing the chattering induced by discontinuous control actions [23]. This innovation has fostered the application of fractional-order methodologies in a multitude of nonlinear control systems, including tailored solutions for spacecraft attitude control. Alipour et al.'s [24] work introduced an adaptive fractional-order nonsingular terminal SMC, ingeniously designed to stabilize spacecraft attitude while concurrently minimizing reaction wheel momentum errors. Zhang et al. [25] introduced a novel fault-tolerant control scheme, integrating fractional-order nonsingular terminal sliding mode control with backstepping techniques, tailored to tackle spacecraft attitude control amidst faults. This strategy ensures the finite-time stability of the tracking error in a faulty closed-loop attitude control system. Qian et al. [26] employed an adaptive sliding mode observer for fault estimation and combined fractional-order SMC with adaptive fuzzy approximation techniques, which ensured enhanced robustness and fault tolerance of the system. Fractional-order control, as elucidated in various seminal works, augments the parameter tuning range, thereby enhancing the flexibility in controller design and refining system response precision [27]. These studies have devised fractional-order SMC for spacecraft applications, demonstrating the efficacy of this approach.

All the previously mentioned methods have demonstrated their effectiveness. However, they all necessitate prior knowledge of system dynamics, thereby precluding their application in realizing optimal tracking control. Due to this limitation, the interest in reinforcement learning (RL) as a means to achieve control optimization has been rejuvenated. Among the prominent and efficacious RL methodologies, the actor-critic RL stands out [28,29]. The integration of neural networks (NNs) with the actor-critic RL framework has spurred significant advancements in intelligent control techniques and shed light on the approaches to address tracking control challenges [30–34]. Wang et al. [35] proposed an RL-oriented optimal control method that effectively reduces vibration and improves the operational efficiency of unmanned ground vehicles operating in complex and uncertain environments. Similarly, Zheng et al. [36] integrated the actor-critic RL framework into an SMC strategy for precise trajectory tracking in spacecraft, emphasizing the adaptability of RL to intricate aerospace engineering applications.

However, a comprehensive method that combines SMC, fractional-order control, and an actor-critic NN (ACNN) has not been investigated. Therefore, this paper proposes ACNNFOSMC for the attitude control of spacecraft amidst uncertainties and actuator faults. The core novelties and advancements of this study can be encapsulated as follows:

(1) The developed framework includes an ACNN framework to approximate the aggregate of uncertain parameters, disturbances, and actuator faults of spacecraft, thereby facilitating their compensation. Unlike traditional neural network (NN) approximation [37,38], an ACNN-based control scheme enables the derivation of an optimized control policy in real-time, utilizing state information. By leveraging neural networks to learn and compensate for system uncertainties, our method reduces the reliance on computationally intensive model development and fine tuning. The ability to adaptively estimate and respond to uncertainties in real time through neural-network-based learning fosters greater robustness in the control system.

(2) A fractional-order super-twisting control based on a fractional-order sliding mode surface is proposed for spacecraft. Compared with SMC, the proposed fractional-order SMC converts the sharp transformation of control signals into smoother fractional derivatives, effectively suppressing the chattering caused by discontinuous control actions. Compared with super-twisting control, it augments the parameter tuning range, thereby enhancing the flexibility in controller design and improving system response precision.

(3) By merging ACNN with a fractional-order super-twisting SMC, we significantly expedite the system's convergence process while concurrently boosting steady-state ac-

curacy. This fusion represents a pivotal advancement in control system dynamics and responsiveness.

2. Model Description and Preliminaries

2.1. Spacecraft Dynamics

Consider the following notation: Let $\boldsymbol{q}^T = [q_1, q_2, q_3]$ and $\boldsymbol{\omega} = [\omega_1, \omega_2, \omega_3]^T \in R^3$ denote attitude and the angular velocity vector, respectively; let $\boldsymbol{q}_u = \left[q_0, \boldsymbol{q}^T\right]^T \in R^4$ with $\boldsymbol{q}^T\boldsymbol{q} + q_0^2 = 1$ denote the unit quaternion, $\boldsymbol{I}_3 \in R^{3\times 3}$ denote the identity matrix; let $\boldsymbol{q}_{ud} = \left[q_{d0}, \boldsymbol{q}_d^T\right]^T \in R^4$ with $\boldsymbol{q}_d^T = [q_{d1}, q_{d2}, q_{d3}]$ and $\boldsymbol{\omega}_d = [\omega_{d1}, \omega_{d2}, \omega_{d3}]^T \in R^3$ denote the desired attitude and angular velocity, respectively; let $\widetilde{\boldsymbol{q}}_u = \left[\widetilde{q}_0, \widetilde{\boldsymbol{q}}^T\right]^T$ and $\widetilde{\boldsymbol{\omega}}$ denote the attitude tracking error and velocity tracking error, respectively. Throughout this document, the index i spans the set $\Omega_i \triangleq \{i : 1, 2, 3\}$; any vector $\boldsymbol{x} \in R^3$ means $\boldsymbol{x} = [x_1, x_2, x_3]^T$, and $\boldsymbol{x}^\times = [0, -x_3, x_2; x_3, 0, -x_1; -x_2, x_1, 0]$ means its skew-symmetric matrix.

The dynamics of spacecraft are formally described by [39]

$$\begin{cases} \dot{q}_0 = -\frac{1}{2}\boldsymbol{q}^T\boldsymbol{\omega},\ \dot{\boldsymbol{q}} = \frac{1}{2}(q_0\boldsymbol{I}_3 + \underline{\boldsymbol{q}}^\times)\boldsymbol{\omega} \\ \boldsymbol{J}\dot{\boldsymbol{\omega}} = -\boldsymbol{\omega}^\times\boldsymbol{J}\boldsymbol{\omega} + \boldsymbol{u} - \boldsymbol{E}\boldsymbol{u} + \boldsymbol{E}\underline{\boldsymbol{u}} + \boldsymbol{d}(t) \end{cases}, \tag{1}$$

where $\boldsymbol{J} = \boldsymbol{J}^T \in R^{3\times 3}$ denotes the inertia matrix, $\underline{\boldsymbol{d}}(t) = [d_1, d_2, d_3]^T \in R^3$ denotes the disturbance, $\boldsymbol{u} \in R^3$ denotes the control torque, $\underline{\boldsymbol{u}} \in R^3$ denotes bounded fault, and $\boldsymbol{E} = \mathrm{diag}\{E_1, E_2, E_3\} \in R^{3\times 3}$ denotes a failure indicator matrix, where its element $0 < E_i \leq 1$ signifies the failure indicator for each respective actuator.

Due to the inherent uncertainty of the inertia matrix, it can be represented as the sum of a nominal inertia matrix $\boldsymbol{J}_0$ and an uncertain component $\Delta\boldsymbol{J}$, expressed as $\boldsymbol{J} = \boldsymbol{J}_0 + \Delta\boldsymbol{J}$. The dynamics (1) are given by

$$\dot{\boldsymbol{\omega}} = -\boldsymbol{J}_0^{-1}\boldsymbol{\omega}^\times\boldsymbol{J}_0\boldsymbol{\omega} + \boldsymbol{J}_0^{-1}\boldsymbol{u} - \boldsymbol{f}_N, \tag{2}$$

where $\boldsymbol{f}_N = \Delta\widetilde{\boldsymbol{J}}\boldsymbol{\omega}^\times\boldsymbol{J}\boldsymbol{\omega} + \boldsymbol{J}_0^{-1}\boldsymbol{\omega}^\times\Delta\boldsymbol{J}\boldsymbol{\omega} - \Delta\widetilde{\boldsymbol{J}}\boldsymbol{u} - \boldsymbol{J}^{-1}\left(\boldsymbol{d}(t) + \boldsymbol{E}\boldsymbol{u} - \boldsymbol{E}\underline{\boldsymbol{u}}\right)$

$\Delta\widetilde{\boldsymbol{J}} = -\boldsymbol{J}_0^{-1}\Delta\boldsymbol{J}\left(\boldsymbol{I}_3 + \boldsymbol{J}_0^{-1}\Delta\boldsymbol{J}\right)\boldsymbol{J}_0^{-1}$.

From Equation (1), it follows that

$$\begin{array}{l} \widetilde{\boldsymbol{q}} = q_{0d}\boldsymbol{q} - \boldsymbol{q}_d^\times\boldsymbol{q} - q_0\boldsymbol{q}_d \\ \widetilde{q}_0 = \boldsymbol{q}_d^T\boldsymbol{q} + q_0q_{0d} \\ \widetilde{\boldsymbol{\omega}} = \boldsymbol{\omega} - \boldsymbol{C}\boldsymbol{\omega}_d \end{array}, \tag{3}$$

where $\boldsymbol{C} = \frac{1}{2}\left(\widetilde{q}_0^2 - \widetilde{\boldsymbol{q}}^T\widetilde{\boldsymbol{q}}\right)\boldsymbol{I}_3 + 2\widetilde{\boldsymbol{q}}^T\widetilde{\boldsymbol{q}} - 2\widetilde{q}_0\widetilde{\boldsymbol{q}}^\times$.

By employing Equations (1)–(3), the description of the tracking error's dynamic behavior is thereby established as

$$\begin{cases} \dot{\widetilde{q}}_0 = -\frac{1}{2}\widetilde{\boldsymbol{q}}^T\widetilde{\boldsymbol{\omega}},\ \dot{\widetilde{\boldsymbol{q}}} = \frac{1}{2}\left(\widetilde{q}_0\boldsymbol{I}_3 + \widetilde{\boldsymbol{q}}^\times\right)\widetilde{\boldsymbol{\omega}} \\ \dot{\widetilde{\boldsymbol{\omega}}} = -\boldsymbol{J}_0^{-1}\boldsymbol{\omega}^\times\boldsymbol{J}_0\boldsymbol{\omega} + \widetilde{\boldsymbol{\omega}}^\times\boldsymbol{C}\boldsymbol{\omega}_d - \boldsymbol{C}\dot{\boldsymbol{\omega}}_d + \boldsymbol{J}_0^{-1}\boldsymbol{u} - \boldsymbol{f}_N \end{cases}, \tag{4}$$

Assumption 1 ([20,21]). *The overall perturbation $\boldsymbol{f}_N$ exhibits continuous differentiability in relation to time.*

2.2. Preliminaries

Within this section, the fundamental concepts pertinent to fractional-order calculus are outlined.

Definition 1 ([22]). *The Riemann–Liouville β-order fractional derivative and integral are expressed as*

$$ {}_a\mathscr{D}_t^{\beta} f(t) = \frac{d^{\beta} f(t)}{dt^{\beta}} = \frac{1}{\Gamma(r-\beta)} \frac{d^r}{dt^r} \int_a^t \frac{f(\tau)}{(t-\tau)^{\beta-r+1}} d\tau, \tag{5} $$

$$ {}_a\mathscr{D}_t^{-\beta} f(t) = {}_a\mathscr{I}_t^{\beta} f(t) = \frac{1}{\Gamma(\beta)} \int_a^t \frac{f(\tau)}{(t-\tau)^{1-\beta}} d\tau, \tag{6} $$

where $f(t)$ denotes any function, $\mathscr{D}^{\beta}$ denotes the fractional derivative, $\mathscr{I}^{\beta}$ represents the fractional integral, $r-1 < \beta < r$, $\Gamma(\cdot)$ is Euler's gamma function, which is given by

$$ \Gamma(\beta) = \int_a^{\infty} e^{-t} t^{\beta-1} dt, \tag{7} $$

Shifting focus to the realm of engineering and control, the prevalent Caputo interpretation for β-order fractional calculus is encapsulated by:

$$ {}_a\mathscr{D}_t^{\beta} f(t) = \frac{1}{\Gamma(r-\beta)} \int_a^t (t-\tau)^{r-\beta-1} f^{(r)}(\tau) d\tau, \tag{8} $$

Notably, it is important to recognize ${}_a\mathscr{D}_t^{\beta} f(t) = {}_a\mathscr{I}_t^{1-\beta} \dot{f}(t)$ in this context. Nonetheless, the versatility of operator (8) resides in its broad applicability to an extensive set of continuous functions, which may not be restricted to exhibiting solely integer-order derivatives.

3. Controller Design

The control scheme framework proposed in this paper is shown in Figure 1. The integration of an ACNN with a super-twisting SMC with fractional-order theory enables dual functionality: the ACNN serves to approximate the aggregate of uncertain parameters, disturbances, and actuator faults, thereby facilitating their compensation, while the fractional-order super-twisting SMC significantly improves the system's tracking precision and overall robustness against uncertainties.

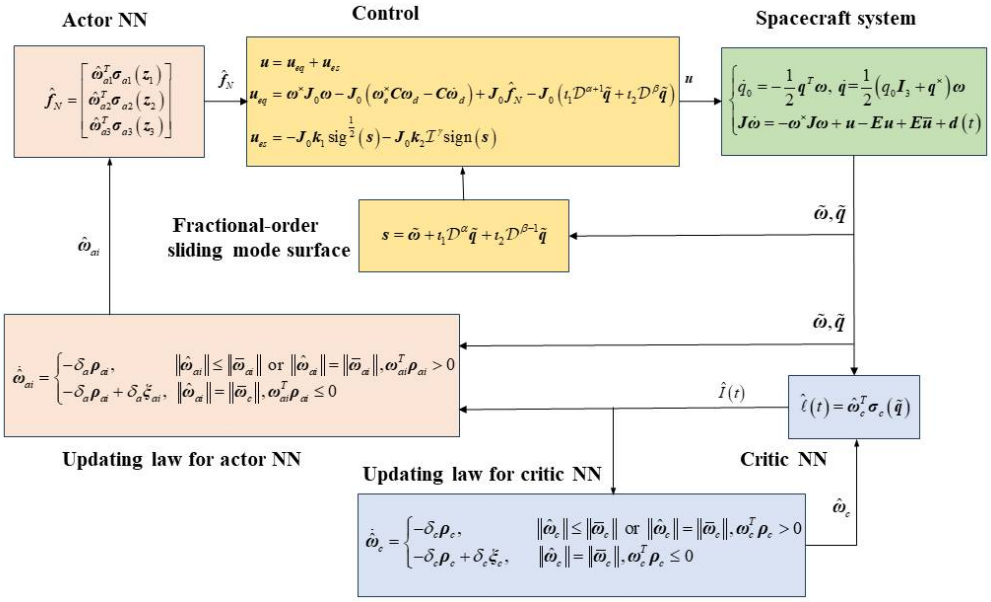


Figure 1. The framework of the proposed control scheme.

3.1. Uncertainty Estimation Using Actor-Critic NN

The unknown and time-varying nature of f_N has an impact on control efficacy. To address this, f_N can be approximated using an ACNN.

3.1.1. Critic NN

The unknown and time-varying nature of f_N, has an impact on control efficacy. To address this, f_N can be approximated using an ACNN.

Regarding the critic NN, a long-term cost function can be formulated as [28]

$$\ell(t) = \int_t^{\infty} e^{-\frac{\tau - t}{\psi}} \eta(\tau) d\tau, \tag{9}$$

where ψ serves as a constant factor for discounting the future cost, and $\eta(t)$ denotes an instant cost function given by

$$\varphi(t) = \widetilde{\boldsymbol{q}}^T \boldsymbol{M} \widetilde{\boldsymbol{q}} + \boldsymbol{u}^T \boldsymbol{G} \boldsymbol{u}, \tag{10}$$

where $\boldsymbol{M}$ and $\boldsymbol{G}$ denote the designed positive definite matrices. The pinnacle of control performance is attained upon achieving the minimal accumulated cost, referred to as the cost-to-go function.

Based on the approximation property of NNs, $\ell(t)$ can be represented as $\ell(t) = \boldsymbol{\omega}_c^{*T} \boldsymbol{\sigma}_c(\widetilde{\boldsymbol{q}}) + \varepsilon_c$, where $\boldsymbol{\omega}_c^* = \left[\omega_{c1}^*, \omega_{c2}^*, \cdots, \omega_{ch}^*\right]^T$ signifies the vector of optimal weights, h indicates the quantity of nodes comprising the hidden layer, $\widetilde{\boldsymbol{q}} = [\widetilde{q}_1, \widetilde{q}_2, \widetilde{q}_3]^T$ characterizes the input vector, ε_c is referred to as the least approximation error, and $\sigma_c(\widetilde{\boldsymbol{q}})$ utilizes a Gaussian function structured as

$$\boldsymbol{\sigma}_c(\widetilde{\boldsymbol{q}}) = \exp\left[-\left(\widetilde{\boldsymbol{q}} - \mu_{cj}\right)^T \left(\widetilde{\boldsymbol{q}} - \mu_{cj}\right) / b_{cj}^2\right], j = 1, 2, \cdots, h, \tag{11}$$

where $\mu_{cj} = \left[\mu_{cj1}, \mu_{cj2}, \mu_{cj3}\right]^T$ signifies the receptive field's centroid, and b_{cj} denotes the breadth of the Gaussian function.

The approximation for $\ell(t)$ is formalized by

$$\hat{\ell}(t) = \hat{\boldsymbol{\omega}}_c^T \boldsymbol{\sigma}_c(\widetilde{\boldsymbol{q}}), \tag{12}$$

With respect to Equations (10) and (12), the approximate error of the cost function is expressed as

$$\lambda(t) = \eta(t) - \frac{1}{\psi} \hat{\ell}(t) + \dot{\hat{\ell}}(t), \tag{13}$$

To outline the update rule for the critic NN, $E_c = (1/2)\lambda^2$ is defined. Based on the principle of gradient descent, the adjustment rule for the critic network's weights is devised as

$$\dot{\hat{\boldsymbol{\omega}}}_c = -\delta_c \frac{\partial E_c}{\partial \hat{\boldsymbol{\omega}}_c}, \tag{14}$$

Upon integrating Equation (13) into Equation (14), the resultant expression becomes

$$\begin{aligned} \dot{\hat{\boldsymbol{\omega}}}_c &= -\delta_c \lambda \frac{\partial E_c}{\partial \hat{\boldsymbol{\omega}}_c} \\ &= -\delta_c \lambda \frac{\partial \left[\eta(t) - (1/\psi)\hat{\ell}(t) + \dot{\hat{\ell}}(t)\right]}{\partial \hat{\boldsymbol{\omega}}_c} \\ &= -\delta_c \lambda \left[-\frac{1}{\psi} \frac{\partial \hat{\ell}}{\partial \hat{\boldsymbol{\omega}}_c} + \frac{\partial}{\partial \hat{\boldsymbol{\omega}}_c} \left(\frac{\partial \hat{\ell}}{\partial \widetilde{\boldsymbol{q}}}\right) \dot{\widetilde{\boldsymbol{q}}}\right] \end{aligned}, \tag{15}$$

where δ_c signifies the learning rate of the critic NN.

Defining $\boldsymbol{\zeta}_c\left(\hat{\boldsymbol{\omega}}_c, \widetilde{\boldsymbol{q}}, \dot{\widetilde{\boldsymbol{q}}}\right) = \left(\eta(t) + \hat{\boldsymbol{\omega}}_c^T \boldsymbol{\Lambda}\right)\boldsymbol{\Lambda}$ with $\boldsymbol{\Lambda} = -(\sigma_c/\psi) + \nabla\sigma_c\dot{\widetilde{\boldsymbol{q}}}$, Equation (15) is further written as

$$\dot{\hat{\boldsymbol{\omega}}}_c = -\delta_c \boldsymbol{\zeta}_c\left(\hat{\boldsymbol{\omega}}_c, \widetilde{\boldsymbol{q}}, \dot{\widetilde{\boldsymbol{q}}}\right), \tag{16}$$

A constant vector $\boldsymbol{\omega}_{c\max} = [\omega_{c\max 1}, \omega_{c\max 2}, \cdots, \omega_{c\max h}]^T$ is selected to adhere to the condition $\left|\hat{\omega}_{cj}\right| \leq \left|\omega_{c\max j}\right|, j = 1, 2, \cdots, h$. To ensure that the critic NN's weights are bounded, an update rule grounded in the projection methodology for the critic NN is formulated as follows:

$$\dot{\hat{\boldsymbol{\omega}}}_c = \begin{cases} -\delta_c \boldsymbol{\zeta}_c, & \|\hat{\boldsymbol{\omega}}_c\| \leq \|\boldsymbol{\omega}_{c\max}\| \text{ or } \|\hat{\boldsymbol{\omega}}_c\| = \|\boldsymbol{\omega}_{c\max}\|, \boldsymbol{\omega}_c^T \boldsymbol{\zeta}_c > 0 \\ -\delta_c \boldsymbol{\zeta}_c + \delta_c \boldsymbol{\xi}_c, & \|\hat{\boldsymbol{\omega}}_c\| = \|\boldsymbol{\omega}_{c\max}\|, \boldsymbol{\omega}_c^T \boldsymbol{\zeta}_c \leq 0 \end{cases}, \tag{17}$$

where $\boldsymbol{\xi}_c = \left(\hat{\boldsymbol{\omega}}_c^T \boldsymbol{\zeta}_c / \|\hat{\boldsymbol{\omega}}_c\|^2\right)\hat{\boldsymbol{\omega}}_c$. Provided that $\|\hat{\boldsymbol{\omega}}_c(0)\| \leq \|\boldsymbol{\omega}_{c\max}\|$ holds true, the implementation of the projection-based update law in Equation (17) consistently upholds the constraint $\|\hat{\boldsymbol{\omega}}_c\| \leq \|\boldsymbol{\omega}_{c\max}\|$.

3.1.2. Actor NN

The output vector $\hat{\boldsymbol{f}}_N$ of radial basis function NN, which serves to approximate modeling uncertainties $\boldsymbol{f}_N$, is formulated as

$$\hat{\boldsymbol{f}}_N = \begin{bmatrix} \hat{\boldsymbol{\omega}}_{a1}^T \boldsymbol{\sigma}_{a1}(\boldsymbol{z}_1) \\ \hat{\boldsymbol{\omega}}_{a2}^T \boldsymbol{\sigma}_{a2}(\boldsymbol{z}_2) \\ \hat{\boldsymbol{\omega}}_{a3}^T \boldsymbol{\sigma}_{a3}(\boldsymbol{z}_3) \end{bmatrix}, \tag{18}$$

where $\boldsymbol{\omega}_{ai} = [\omega_{ai1}, \omega_{ai2}, \cdots, \omega_{aim}]^T$, $\boldsymbol{\sigma}_{ai}(\boldsymbol{z}_i)$ and $\boldsymbol{z}_i = [\widetilde{q}_{1i}, \widetilde{\omega}_{1i}]^T$ represent the weight vector, the Gaussian function, and the input vector, respectively.

The approximate error of the actor NN is expressed as

$$\widetilde{f}_{Ni} = \widetilde{\boldsymbol{\omega}}_{ai}^T \boldsymbol{\sigma}_{ai}(\boldsymbol{z}_i), \tag{19}$$

where $\widetilde{\boldsymbol{\omega}}_{ai} = \boldsymbol{\omega}_{ai}^* - \hat{\boldsymbol{\omega}}_{ai}$. Considering Equations (9) and (12), let $\ell_d(t) = 0$ represent the expected cost function for future states; the error associated with actor NN is given by

$$e_a = \widetilde{f}_{Ni} + k_\ell\left(\hat{\ell}(t) - \ell_d(t)\right), \tag{20}$$

where $k_\ell > 0$ is a coefficient. Upon defining $E_a = \ln(\cosh(e_a))$, the updating rule of the actor NN's weights is devised as

$$\begin{aligned} \dot{\hat{\boldsymbol{\omega}}}_{ai} &= -\delta_a \tfrac{\partial E_a}{\partial \hat{\boldsymbol{\omega}}_a} \\ &= -\delta_a \tfrac{dE_a}{de_a} \tfrac{\partial e_a}{\partial \widetilde{f}_{Ni}} \tfrac{\partial \widetilde{f}_{Ni}}{\partial \widetilde{\boldsymbol{\omega}}_{ai}} \\ &= -\delta_a \tanh\left(\widetilde{f}_{Ni} + k_\ell \hat{\ell}\right)\boldsymbol{\sigma}_{ai} \end{aligned}, \tag{21}$$

where δ_a is the designed updating rate. In light of the unavailability of $\widetilde{f}_{Ni}$, Equation (21) is modified as follows:

$$\begin{aligned} \dot{\hat{\boldsymbol{\omega}}}_{ai} &= -\delta_a \tanh\left(\sum_{i=1}^{n} \hat{\boldsymbol{\omega}}_{ai}^T \boldsymbol{\sigma}_{ai} + k_\ell \hat{\ell}\right)\boldsymbol{\sigma}_{ai} \\ &= -\delta_a \boldsymbol{\zeta}_{ai}\left(\hat{\boldsymbol{\omega}}_{ai}, \widetilde{\boldsymbol{q}}, \dot{\widetilde{\boldsymbol{q}}}\right) \end{aligned}, \tag{22}$$

To ensure that the actor NN's weights are bounded, parameter projection is employed. A set of constant vectors $\boldsymbol{\omega}_{ai\max} = [\omega_{ai1\max}, \omega_{ai2\max}, \cdots, \omega_{aih\max}]^T$ are tailored to fulfill the

condition $\left|\hat{\omega}_{aij}\right| \leq \left|\omega_{aij\max}\right| (j = 1, 2, \cdots, h)$, leading to the design of a projection-based update law for the actor NN as follows:

$$\dot{\hat{\boldsymbol{\omega}}}_{ai} = \begin{cases} -\delta_a \boldsymbol{\zeta}_{ai}, & \|\hat{\boldsymbol{\omega}}_{ai}\| \leq \|\boldsymbol{\omega}_{ai\max}\| \text{ or } \|\hat{\boldsymbol{\omega}}_{ai}\| = \|\boldsymbol{\omega}_{ai\max}\|, \boldsymbol{\omega}_{ai}^T \boldsymbol{\zeta}_{ai} > 0 \\ -\delta_a \boldsymbol{\zeta}_{ai} + \delta_a \boldsymbol{\xi}_{ai}, & \|\hat{\boldsymbol{\omega}}_{ai}\| = \|\boldsymbol{\omega}_{ai\max}\|, \boldsymbol{\omega}_{ai}^T \boldsymbol{\zeta}_{ai} \leq 0 \end{cases}, \tag{23}$$

where $\boldsymbol{\xi}_{ai} = \left(\hat{\boldsymbol{\omega}}_{ai}^T \boldsymbol{\zeta}_{ai} / \|\hat{\boldsymbol{\omega}}_{ai}\|^2\right) \hat{\boldsymbol{\omega}}_{ai}$. Provided that $\|\hat{\boldsymbol{\omega}}_{ai}(0)\| \leq \|\boldsymbol{\omega}_{ai\max}\|$ holds true, the projection updating law (23) consistently guarantees the constraint $\|\hat{\boldsymbol{\omega}}_{ai}\| \leq \|\boldsymbol{\omega}_{ai\max}\|$.

3.2. Fractional-Order Super-Twisting Sliding Mode Control

A fractional-order sliding mode surface is configured as

$$\boldsymbol{s} = \widetilde{\boldsymbol{\omega}} + \iota_1 \mathscr{D}^{\alpha} \widetilde{\boldsymbol{q}} + \iota_2 \mathscr{D}^{\beta - 1} \widetilde{\boldsymbol{q}}, \tag{24}$$

where ι_1 and ι_2 denote coefficients, $0 \leq \alpha \leq 1$, and $0 \leq \beta \leq 1$.

Derived from Equation (24), the dynamics of $\boldsymbol{s}$ are delineated by

$$\begin{array}{rl} \dot{\boldsymbol{s}} & = \dot{\widetilde{\boldsymbol{\omega}}} + \iota_1 \mathscr{D}^{\alpha+1} \widetilde{\boldsymbol{q}} + \iota_2 \mathscr{D}^{\beta} \widetilde{\boldsymbol{q}} \\ & = -\boldsymbol{J}_0^{-1} \boldsymbol{\omega}^{\times} \boldsymbol{J}_0 \boldsymbol{\omega} + \widetilde{\boldsymbol{\omega}}^{\times} \boldsymbol{C} \boldsymbol{\omega}_d - \boldsymbol{C} \dot{\boldsymbol{\omega}}_d + \boldsymbol{J}_0^{-1} \boldsymbol{u} \\ & -\hat{\boldsymbol{f}}_N + \boldsymbol{\varepsilon} + \iota_1 \mathscr{D}^{\alpha+1} \widetilde{\boldsymbol{q}} + \iota_2 \mathscr{D}^{\beta} \widetilde{\boldsymbol{q}} \end{array}, \tag{25}$$

From Equation (25), the control law is thereby formulated as

$$\begin{array}{rcl} \boldsymbol{u} & = & \boldsymbol{u}_{eq} + \boldsymbol{u}_{es} \\ \boldsymbol{u}_{eq} & = & \boldsymbol{\omega}^{\times} \boldsymbol{J}_0 \boldsymbol{\omega} - \boldsymbol{J}_0 \left(\boldsymbol{\omega}_e^{\times} \boldsymbol{C} \boldsymbol{\omega}_d - \boldsymbol{C} \dot{\boldsymbol{\omega}}_d\right) + \boldsymbol{J}_0 \hat{\boldsymbol{f}}_N - \boldsymbol{J}_0 \left(\iota_1 \mathscr{D}^{\alpha+1} \widetilde{\boldsymbol{q}} + \iota_2 \mathscr{D}^{\beta} \widetilde{\boldsymbol{q}}\right) \\ \boldsymbol{u}_{es} & = & -\boldsymbol{J}_0 \boldsymbol{k}_1 \mathrm{sig}^{\frac{1}{2}}(\boldsymbol{s}) - \boldsymbol{J}_0 \boldsymbol{k}_2 \mathscr{I}^{\gamma} \mathrm{sign}(\boldsymbol{s}) \end{array}, \tag{26}$$

where $0 < \gamma \leq 1$.

Remark 1. *When $\gamma = 1$, the fractional-order control scheme (26) is transformed into the classical integer-order super-twisting controller, whose control performance and stability characteristics have been extensively investigated in many prior studies. Consequently, the present discussion intentionally excludes the case where $\gamma = 1$, focusing exclusively on the cases where $0 < \gamma < 1$.*

Incorporating Equation (26) into Equation (25) leads to

$$\dot{\boldsymbol{s}} = -\boldsymbol{k}_1 \mathrm{sig}^{\frac{1}{2}}(\boldsymbol{s}) - \boldsymbol{k}_2 \mathscr{I}^{\gamma} \mathrm{sign}(\boldsymbol{s}) + \boldsymbol{f}_d, \tag{27}$$

where $\boldsymbol{f}_d = \widetilde{\boldsymbol{f}}_N + \boldsymbol{\varepsilon}, \widetilde{\boldsymbol{f}}_N = \boldsymbol{f}_N - \hat{\boldsymbol{f}}_N$.

Subsequently, Equation (27) can be reformulated as

$$\begin{array}{l} \dot{\boldsymbol{s}} = -\boldsymbol{k}_1 \mathrm{sig}^{\frac{1}{2}}(\boldsymbol{s}) + \boldsymbol{s}_I \\ \mathscr{D}^{\gamma} \boldsymbol{s}_I = -\boldsymbol{k}_2 \mathrm{sign}(\boldsymbol{s}) + \dot{\boldsymbol{f}}_d \end{array}, \tag{28}$$

For clarity and comprehension, Equation (28) is recast in scalar format as:

$$\begin{array}{l} \dot{s}_i = -k_{1i} \mathrm{sig}^{\frac{1}{2}}(s_i) + s_{Ii} \\ \mathscr{D}^{\gamma} s_{Ii} = -k_{2i} \mathrm{sign}(s_i) + \dot{f}_{di} \end{array}, \tag{29}$$

The sequence $(t_n)_{n \in N \cup \{0\}}$, which is characterized by strict monotonic increase, comprises every instant fulfilling the criterion $s_i(t_n) = 0$. The presence of solutions to Equation (29) is elucidated following Garrappa's [40] framework, thereby augmenting the Filippov regularization methodology to encompass fractional-order scenarios. Capitalizing

on the implications derived from Equation (29), particularly with regard to $\dot{s}_i(t_n) = s_{Ii}(t_n)$, Equation (25) undergoes a transformation into its subsequent form

$$\dot{s}_i(t) = \dot{s}_i(t_n) - k_{1i}\mathrm{sig}^{\frac{1}{2}}(s_i) - k_{2i}\mathscr{I}^{\gamma}\mathrm{sign}(s_i) + \mathscr{I}^{\gamma}\dot{f}_{di}(t), \tag{30}$$

Based on Assumption 1 and the characteristics of neural networks, we can assume that $\dot{f}_{di}(t)$ is bounded.

4. Stability Analysis

Theorem 1. *Given the dynamics during the reaching phase described in Equation (30) with* $\gamma/(\gamma+1) < 0.5$ *and* $\gamma \in (0,1)$*, if the parameters are selected to meet the following constraints*

$$\begin{aligned} &k_{1i} > 0 \\ &k_{2i} > \max\left(\tfrac{3+\gamma}{1-\gamma}\delta_m, \left(\tfrac{k_{1i}}{1-\varsigma}\right)^{\gamma/0.5}|s_{Ii}(t_0)|^{1-\gamma} + \delta_m\right) \\ &\varsigma = (1+\gamma)(k_{2i}+\delta_m)/(k_{2i}-\delta_m) - 1 < 1 \end{aligned}, \tag{31}$$

then there exists a finite time $t = t_f$ *where* $s_i(t) = s_{Ii}(t) = 0$ *holds for* $t \geq t_f$*, where* $t_f \leq t_0 + \dfrac{1}{1-\mu_s^{1/\gamma}}\sum\limits_{n=0}^{\infty}\left[\mu_s^n \dfrac{\Gamma(2+\gamma)}{k_{2i}-\delta_{im}} s_{Ii}(t_0)\right]^{1/\gamma}$*, which applies for* $\mu_s = \varsigma + \dfrac{k_{1i}|s_{Ii}(t_0)|^{0.5(1+1/\gamma)-1}}{(1+1/\gamma)^{0.5}}\left[\dfrac{\Gamma(2+\gamma)}{k_{2i}-\delta_{im}}\right]^{0.5/\gamma} < 1$ *and commences with the given initial conditions* $(s_i(t), s_{Ii}(t)) = (0,0)$.

Proof of Theorem 1. For a detailed proof, readers are referred to [40]. Consider an open interval (t_0, t_1) and assume $s_i(t) = s_{Ii}(t) = 0$, then $\dot{\phi}_1(t) \leq \dot{s}_i(t) \leq \dot{\phi}_2(t)$, $\phi_1(t) \leq s_i(t) \leq \phi_2(t)$. $\phi_1(t)$, and $\phi_2(t)$ are given by

$$\begin{aligned} \phi_1(t) &= s_{Ii}(t_0)(t-t_0) - \lambda_M \phi_{2M}^{0.5}(t-t_0) - \tfrac{k_{2i}+\delta_{im}}{\Gamma(2+\gamma)}(t-t_0)^{1+\gamma} \\ \phi_2(t) &= s_{Ii}(t_0)(t-t_0) - \tfrac{k_{2i}-\delta_{im}}{\Gamma(2+\gamma)}(t-t_0)^{1+\gamma} \end{aligned}, \tag{32}$$

where $\phi_{2M} = \sup\phi_2(t)$.

To ascertain an upper limit for time t_1, for which $s_i(t_1) = 0$, consider $t = t_{\phi_2}$ as the time at $\phi_2(t_{\phi_2}) = 0$ since $t_1 \leq t_{\phi_2}$, which leads to

$$(t-t_0)^{\gamma} \leq (t_{\phi_2} - t_0)^{\gamma} = \frac{\Gamma(2+\gamma)}{k_{2i}-\delta_{im}} s_{Ii}(t_0), \tag{33}$$

Additionally, in the scenario where $\phi_2(t'_{\phi_2}) = \phi_{2M}$, with t'_{ϕ_2} marking the instance when $\dot{\phi}_2(t'_{\phi_2}) = 0$, the following holds

$$(t'_{\phi_2} - t_0)^{\gamma} = \frac{\Gamma(1+\gamma)}{k_{2i}-\delta_{im}} s_{Ii}(t_0), \tag{34}$$

One obtains

$$\phi_{2M}^{0.5} = \frac{[s_{Ii}(t_0)]^{0.5(1+1/\gamma)}}{(1+1/\gamma)^{0.5}}\left[\frac{\Gamma(1+\gamma)}{k_{2i}-\delta_{im}}\right]^{0.5/\gamma}, \tag{35}$$

$t_1 \leq t_{\phi_2}$ and the monotonically decreasing nature of $\dot{\phi}_1(t)$ ensure that $\dot{\phi}_1(t_{\phi_2}) \leq s_{Ii}(t_1)$, where $\dot{\phi}_1(t_{\phi_2}) = -\mu_s s_{Ii}(t_0)$. Therefore, $-\mu_s s_{Ii}(t_0) \leq s_{Ii}(t_1) < 0$ holds, equivalently

$$|s_{Ii}(t_1)| \leq \mu_s |s_{Ii}(t_0)|, \tag{36}$$

Next, with the assumption $|s_{Ii}(t_m)| \leq \mu_s^m |s_{Ii}(t_0)|$ being valid for the first $m \in \{1, \cdots, n\}$ and solving in (t_n, t_{n+1}), it follows that

$$\begin{aligned} \frac{|s_{Ii}(t_{n+1})|}{|s_{Ii}(t_n)|} &\leq \varsigma + \frac{k_{1i}|s_{Ii}(t_n)|^{0.5(1+1/\gamma)-1}}{(1+1/\gamma)^{0.5}} \left[\frac{\Gamma(1+\gamma)}{k_{2i}-\delta_{im}}\right]^{0.5/\gamma} \\ &\leq \varsigma + \frac{k_{1i}|s_{Ii}(t_0)|^{0.5(1+1/\gamma)-1}}{(1+1/\gamma)^{0.5}} \left[\frac{\Gamma(1+\gamma)}{k_{2i}-\delta_{im}}\right]^{0.5/\gamma} \\ &= \mu_s \end{aligned}, \tag{37}$$

From Equation (37), one has $|s_{Ii}(t_{n+1})| \leq \mu_s^{n+1}|s_{Ii}(t_0)|$, which leads to $\lim_{n\to\infty} s_{Ii}(t_n) = 0$. Considering $(t_{n+1} - t_n)^\gamma = \mu_s^n \frac{\Gamma(2+\gamma)}{k_{2i}-\delta_{im}} s_{Ii}(t_0)$, an estimation for the time to convergence is derived as

$$\begin{aligned} t_f &= t_0 + \sum_{n=0}^{\infty} (t_{n+1} - t_n) \\ &\leq t_0 + \sum_{n=0}^{\infty} \left[\mu_s^n \frac{\Gamma(2+\gamma)}{k_{2i}-\delta_{im}} s_{Ii}(t_0)\right]^{1/\gamma} \\ &\leq t_0 + \frac{1}{1-\mu_s^{1/\gamma}} \sum_{n=0}^{\infty} \left[\mu_s^n \frac{\Gamma(2+\gamma)}{k_{2i}-\delta_{im}} s_{Ii}(t_0)\right]^{1/\gamma} \end{aligned} \tag{38}$$

Consequently, at $t = t_f$, $s_{Ii}(t) = 0$ holds, persisting for any subsequent instant t_f. Moreover, assuming the existence of a time $t' > t_f$ where $s_i(t') \neq 0$ yields to a contradiction, this serves to validate that $s_i(t) = s_{Ii}(t) = 0 \; \forall t \geq t_f$.□

5. Simulations

In this study, we present a novel ACNNFOSMC aimed at enhancing the performance of spacecraft systems under disturbances, uncertainties, and faults. To validate the efficacy and superiority of our proposed method, comprehensive simulations were conducted, with fractional-order PID (FOPID) and smooth super-twisting SMC (SSTSMC) [20] selected as benchmarks for comparison. For the selection of system parameters, we mainly referred to [20]. The main parameter of the system is inertia. The nominal inertia of the spacecraft was $\boldsymbol{J}_0 = \text{diag}\{21, 18, 15\}$ kg·m^2; inertia uncertainties were set as $\Delta\boldsymbol{J} = [2\sin(0.1t), 1.3, 0.8; 1.0, 2\sin(0.2t), 1.5; 0.9, 1.5, \sin(0.3t)]$ kg·m^2. Within these simulations, the disturbances were set as $\boldsymbol{d}(t) = [0.8\sin(0.1t), 0.4\sin(0.2t), 0.3\sin(0.5t)]$ N·m, fault signals were set as $\overline{u}_i = \begin{cases} 0, t \leq 25 \text{ s} \\ 0.2 + 0.1\sin(5t), t > 25 \text{ s} \end{cases}$ and $E_i = \begin{cases} 0, t \leq 20 \text{ s} \\ 0.2, t > 20 \text{ s} \end{cases}$, the expected signal were given by $\boldsymbol{q}_d(0) = [1, 0, 0, 0]^T$ and $\boldsymbol{\omega}_d = 0.06 \times [\sin(\pi t/80), \cos(2\pi t/80), \sin(3\pi t/80)]^T$, and the initial states were set as $\boldsymbol{q} = [0.8832, 0.3, -0.2, -0.3]^T$ and $\boldsymbol{\omega} = [0.1, -0.04, 0.03]^T$. The control gains of ACNNFOSMC were set as $\iota_1 = \iota_2 = 0.1$, $\mu_{cj} = -5 : 0.5 : 5$, $b_{cj} = 0.1$, $\delta_c = 2$, $\mu_{aj} = -5 : 0.2 : 5$, $b_{aj} = 1$, $\delta_c = 4$, $\boldsymbol{k}_1 = 260$, and $\boldsymbol{k}_2 = 10$.

The simulation results, depicted in Figures 2–4, illustrate the attitude and angular velocity tracking performances of the three control strategies. In Figures 2–4, the spacecraft under all three controllers can quickly converge to a stable state in about 15 s. Specifically, the attitude tracking errors for the proposed controller, fractional-order PID, and smooth super-twisting controllers were recorded as $|\widetilde{q}_i| \leq 7.8 \times 10^{-4}$, $|\widetilde{q}_i| \leq 6.2 \times 10^{-3}$, and $|\widetilde{q}_i| \leq 4 \times 10^{-3}$, respectively. Correspondingly, the angular velocity tracking errors stood at $|\widetilde{\omega}_i| \leq 1 \times 10^{-3}$ rad/s, $|\widetilde{\omega}_i| \leq 3 \times 10^{-3}$ rad/s, and $|\widetilde{\omega}_i| \leq 9 \times 10^{-3}$ rad/s. These findings undeniably highlight the superior tracking precision offered by our proposed controller, outperforming the conventional methods in both attitude and angular velocity control tasks.

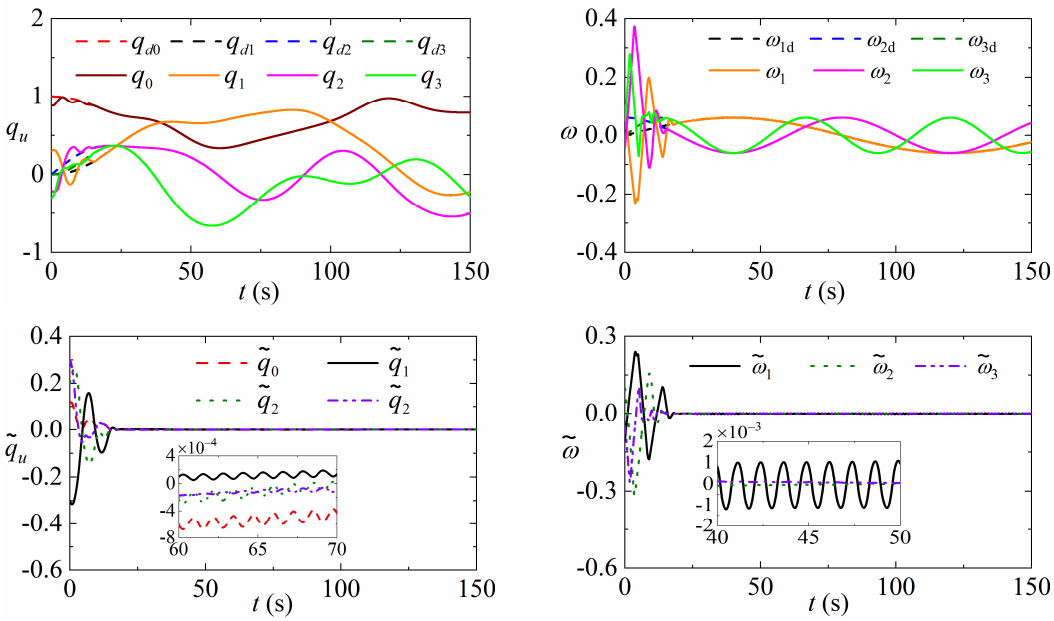


Figure 2. The tracking performance of spacecraft with ACNNFOSMC.

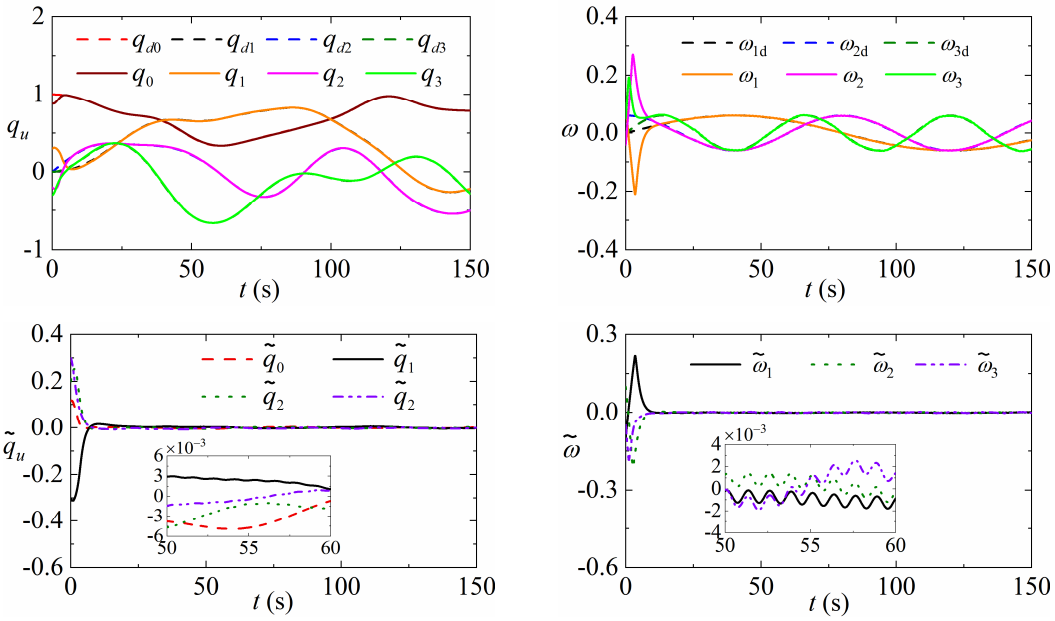


Figure 3. The tracking performance of spacecraft with FOPID.

Figure 5 provides insights into the control input profiles, revealing that despite all controllers maintaining control inputs within the predefined bounds of ±2 Nm, the fractional-order PID control exhibits the smoothest control signal among the three, which is a critical aspect in reducing system wear and improving overall efficiency. This observation underscores the importance of control signal smoothness for practical applications. A unique aspect of our method lies in the adaptive tuning of the actor-critic neural network weights, as illustrated in Figure 6. This figure showcases the self-adaptive process of the neural network's parameters, which dynamically adjusts to optimize control performance, thereby contributing to the robustness and adaptability of the proposed ACNNFOSMC. In conclusion, the proposed ACNNFOSMC has demonstrated remarkable capabilities in terms of tracking accuracy and robustness against various operational challenges.

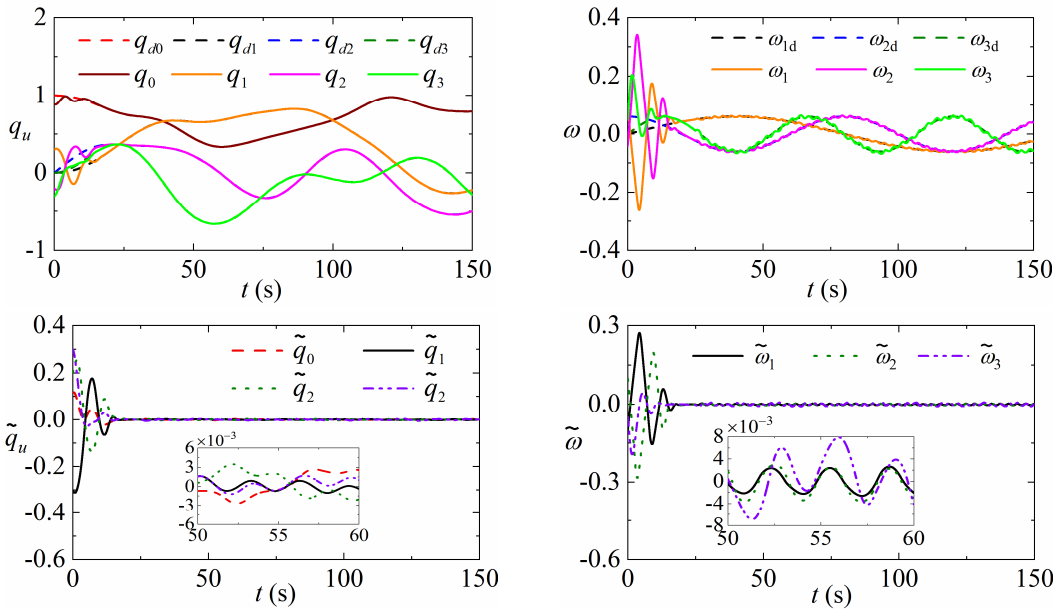


Figure 4. The tracking performance of spacecraft with SSTSMC.

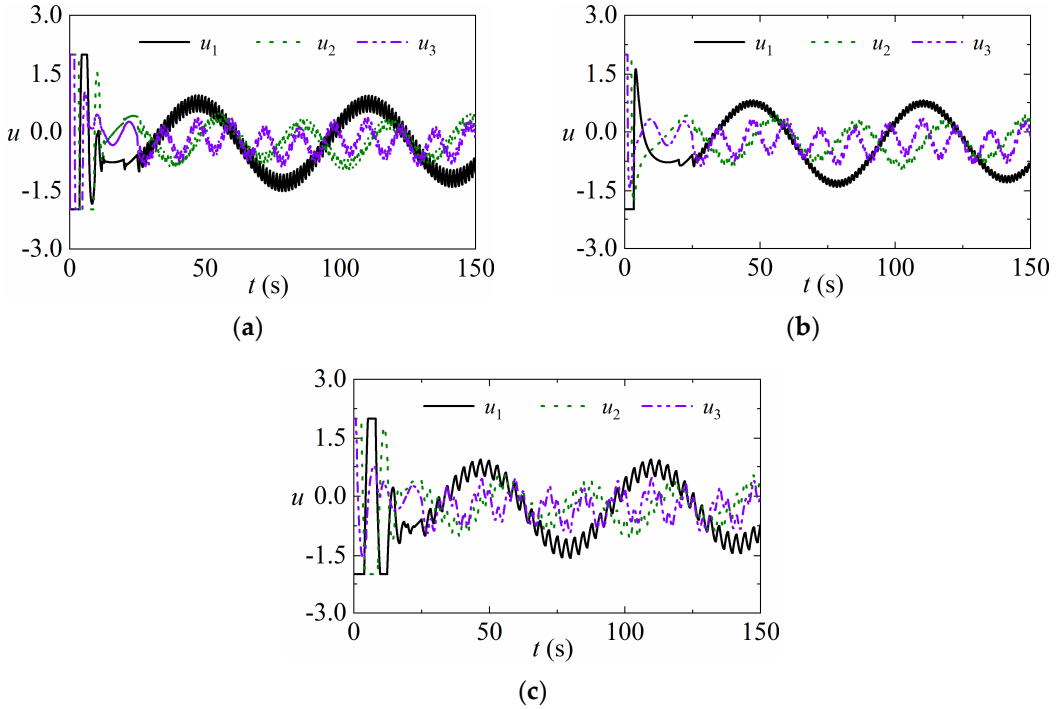


Figure 5. Comparison of control inputs for (**a**) ACNNFOSMC; (**b**) FOPID; (**c**) SSTSMC.

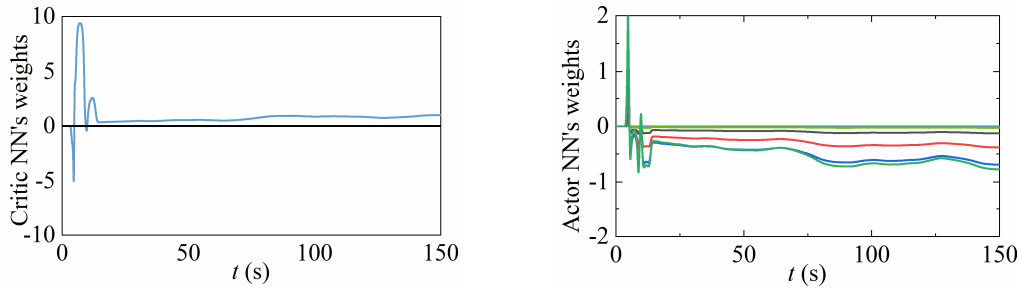


Figure 6. The adaptive tuning of the actor-critic NN's weights.

To further validate the adaptive capability and strong robustness of the proposed control method, the system inertia uncertainty was set to $\Delta \boldsymbol{J}$ = [8 sin (0.1t),2.3,1.8;1.0, 6 sin (0.2t), 2.5;2.9,1.5,8 sin (0.3t)], and the disturbance was configured as $\boldsymbol{d}$ (t) = [1.2 sin (0.2t),0.8 sin (0.3t),0.7 sin (0.5t). Figure 7 illustrates the corresponding attitude and angular velocity tracking errors of the system under the proposed method and classical sliding mode control, while Figure 8 presents the control inputs.

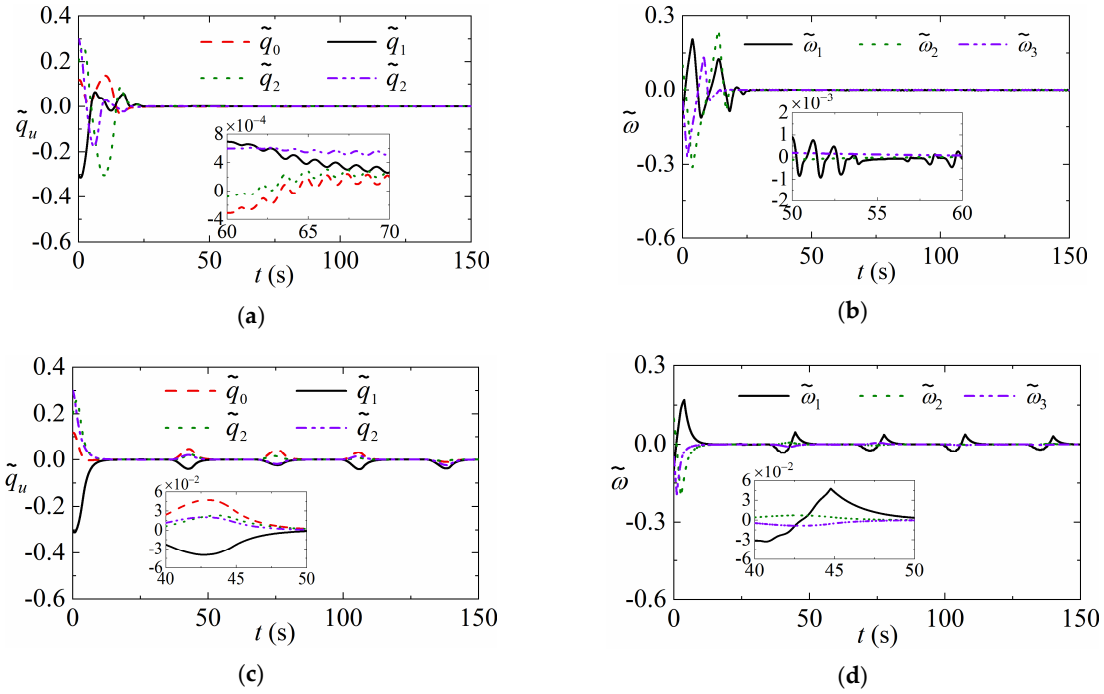


Figure 7. Comparison of tracking performance: (**a**) attitude tracking errors of ACNNFOSMC; (**b**) angular velocity errors of ACNNFOSMC; (**c**) attitude tracking errors of SMC; (**d**) angular velocity errors of SMC.

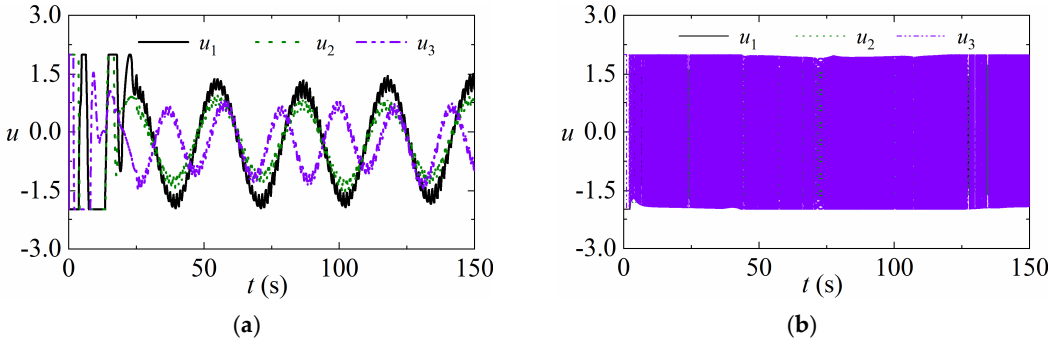


Figure 8. Comparison of control inputs for (**a**) ACNNFOSMC; (**b**) SMC.

Comparing Figures 2 and 7, it is evident that while increases in uncertainties and disturbances lead to a longer time for the system to reach the steady state, under the action of the proposed controller, the system still exhibits minimal attitude tracking errors and angular velocity tracking errors. This demonstrates that the proposed controller possesses strong adaptive capabilities and robustness against disturbances. As shown in Figure 8, compared to sliding mode control, the proposed method effectively suppresses chattering, further highlighting its advantages.

6. Conclusions

This study has successfully investigated and tackled the critical challenge of attitude control for rigid spacecraft under uncertain environments, encountering unpredictable disturbances and facing potential actuator failures. By introducing a novel control strategy that merges the prowess of an actor-critic neural network with the advanced principles of a fractional-order super-twisting sliding mode control, we have demonstrated a significant advancement in spacecraft control systems. The proposed actor-critic neural-network-based fractional-order super-twisting sliding mode control scheme has proven instrumental in accurately estimating and compensating for the combined influence of uncertainties, external disturbances, and actuator faults. The actor-critic neural network has shown exceptional adaptability in the real-time estimation of these detrimental factors, thereby enabling effective countermeasures. Concurrently, the employment of fractional-order control has significantly bolstered the system's responsiveness and precision, ensuring enhanced tracking accuracy and overall system robustness. The stability analyses performed in this research have rigorously substantiated the theoretical foundations of ACNNFOSMC, affirming its ability to maintain system stability amidst varying operational dynamics. The following simulation studies have functioned as concrete evidence, confirming the exceptional efficacy of our proposed methodology. These simulations have illustrated marked improvements in control accuracy and resilience compared to those of other control methods, underlining the practical significance of our control strategy. Given the promising results, ACNNFOSMC emerges as a compelling solution for future spacecraft control systems. It offers a sophisticated yet practical way to navigate complex space environments with uncertainties and hazards. Ultimately, this research underscores the transformative potential of integrating advanced computational intelligence with innovative control theories in advancing aerospace engineering and exploration capabilities. The application of our proposed control strategy is predicated on assumptions of lumped uncertainties that are continuous and bounded in nature. The current limitation is that the tuning of controller parameters necessitates knowledge of the upper bound of these uncertainties, which might pose a practical challenge in some real-world scenarios. By adopting adaptive mechanisms, our future work aims to dynamically adjust controller parameters without the explicit reliance on predefined uncertainty bounds. This adaptive approach would broaden the applicability of our control scheme, enabling it to effectively operate in environments where uncertainty characteristics are less well-known or subject to change over time.

Author Contributions: Methodology, C.J. and X.M.; software, X.M., K.Z. and B.Y.; validation, C.J., K.Z. and B.Y.; formal analysis, C.J., K.Z. and Y.H.; investigation, C.J., X.M., K.Z. and Y.W.; data curation, C.J., X.M. and K.Z.; writing—original draft preparation, C.J., X.M., K.Z. and Y.W.; writing—review and editing, C.J., B.Y. and Y.H; funding acquisition, C.J. and Y.W. All authors have read and agreed to the published version of the manuscript.

Funding: This research was supported in part by the Foundation of Henan University of Technology (No. 2021BS071), the Foundation of the Science and Technology Department of Zhengzhou (No.22ZZRDZX17), and the Key Scientific and Technological Research Projects in Henan Province (No. 242102240039 and No. 232102220085).

Data Availability Statement: Data are contained within the article.

Conflicts of Interest: The authors declare no conflicts of interest.

References

1. Zhang, S.; Zhou, Y.; Cai, S. Fractional-Order PD Attitude Control for a Type of Spacecraft with Flexible Appendages. *Fractal Fract.* **2022**, *6*, 601. [CrossRef]
2. Hasan, M.N.; Haris, M.; Qin, S. Fault-tolerant spacecraft attitude control: A critical assessment. *Prog. Aerosp. Sci.* **2022**, *130*, 100806. [CrossRef]
3. Jin, T.; Kang, G.; Cai, J.; Jia, S.; Yang, J.; Zhang, X.; Liu, F. Disturbance Attenuation and Pointing Control System Design for an Improved Disturbance-Free Payload Spacecraft. *Aerospace* **2023**, *10*, 530. [CrossRef]

4. Golestani, M.; Zhang, W.; Yang, Y.; Xuan-Mung, N. Disturbance observer-based constrained attitude control for flexible spacecraft. *IEEE T. Aero. Elec. Sys.* **2022**, *59*, 963–972. [CrossRef]
5. Jing, C.; Du, H.; Liu, Y. Immersion and invariance based adaptive robust control for attitude tracking of spacecraft with input saturation. *Adv. Space Res.* **2023**, *72*, 3606–3618. [CrossRef]
6. Guo, Y.; Zhou, J.; Liu, Y. Distributed RISE control for spacecraft formation reconfiguration with collision avoidance. *J. Franklin I.* **2019**, *356*, 5332–5352. [CrossRef]
7. Tiwari, M.; Prazenica, R.; Henderson, T. Direct adaptive control of spacecraft near asteroids. *Acta Astronaut.* **2023**, *202*, 197–213. [CrossRef]
8. Nadafi, R.; Kabganian, M. Robust backstepping attitude tracking control of an underactuated spacecraft with saturation and time-variant perturbations. *P. I. Mech. Eng. G-J Aer.* **2022**, *236*, 502–516. [CrossRef]
9. Yao, Q. Robust adaptive iterative learning control for high-precision attitude tracking of spacecraft. *J. Aerospace Eng.* **2021**, *34*, 04020108. [CrossRef]
10. Wang, Z.; Li, Y. Rigid spacecraft nonlinear robust H∞ attitude controller design under actuator misalignments. *Nonlinear Dynam.* **2023**, *111*, 15037–15054. [CrossRef]
11. Pukdeboon, C.; Siricharuanun, P. Nonsingular terminal sliding mode-based finite-time control for spacecraft attitude tracking. *Int. J. Control Autom.* **2014**, *12*, 530–540. [CrossRef]
12. Moradi, R.; Alikhani, A.; Fathi Jegarkandi, M. Spacecraft attitude fault tolerant control based on multi-objective optimization. *J. Theor. App. Mech-Pol.* **2020**, *58*, 983–996. [CrossRef] [PubMed]
13. Hajnorouzali, Y.; Malekzadeh, M.; Ataei, M. Finite-time disturbance observer based-control of flexible spacecraft. *J. Vib. Control* **2023**, *29*, 346–361. [CrossRef]
14. Esmaeilzadeh, S.M.; Golestani, M.; Fekih, A. Adaptive attitude stabilization of flexible spacecraft with fast fixed-time convergence. *IJST-T. Mech. Eng.* **2022**, *46*, 195–208. [CrossRef]
15. Han, Z.; Wang, M.; Yan, X.; Qian, H. Adaptive fixed-time nonsingular terminal sliding mode attitude tracking control for spacecraft with actuator saturations and faults. *Int. J. Aerospace Eng.* **2021**, *1*, 8838784. [CrossRef]
16. Eshghi, S.; Varatharajoo, R. Nonsingular terminal sliding mode control technique for attitude tracking problem of a small satellite with combined energy and attitude control system (CEACS). *Aerosp. Sci. Technol.* **2018**, *76*, 14–26. [CrossRef]
17. Xuan-Mung, N.; Golestani, M. Energy-efficient disturbance observer-based attitude tracking control with fixed-time convergence for spacecraft. *IEEE T. Aero. Elec. Sys.* **2022**, *59*, 3659–3668. [CrossRef]
18. Esmaeilzadeh, S.M.; Golestani, M.; Mobayen, S. Chattering-free fault-tolerant attitude control with fast fixed-time convergence for flexible spacecraft. *Int. J. Control Autom.* **2021**, *19*, 767–776. [CrossRef]
19. Xuan-Mung, N.; Golestani, M.; Hong, S.K. Constrained nonsingular terminal sliding mode attitude control for spacecraft: A funnel control approach. *Mathematics* **2023**, *11*, 247. [CrossRef]
20. Pukdeboon, C. Finite-Time Second-Order Sliding Mode Controllers for Spacecraft Attitude Tracking. *Math. Probl. Eng.* **2013**, 930269. [CrossRef]
21. Lu, K.F.; Xia, Y.Q. Finite-time attitude control for rigid spacecraft-based on adaptive super-twisting algorithm. *IET Control Theory A.* **2014**, *8*, 1465–1477. [CrossRef]
22. Ahmed, S.; Azar, A.T.; Tounsi, M.; Ibraheem, I.K. Adaptive Control Design for Euler–Lagrange Systems Using Fixed-Time Fractional Integral Sliding Mode Scheme. *Fractal Fract.* **2023**, *7*, 712. [CrossRef]
23. Yu, Y.; Liu, X. Model-free fractional-order sliding mode control of electric drive system based on nonlinear disturbance observer. *Fractal Fract.* **2022**, *6*, 603. [CrossRef]
24. Alipour, M.; Malekzadeh, M.; Ariaei, A. Practical fractional-order nonsingular terminal sliding mode control of spacecraft. *ISA T.* **2022**, *128*, 162–173. [CrossRef]
25. Zhang, X.; Gao, Z.; Qian, M.; Bai, L. Integrated fault estimation and fault-tolerant control for rigid spacecraft attitude system with multiple actuator faults. *Int. J. Innov. Comput. I.* **2019**, *15*, 1255–1270.
26. Qian, M.; Shi, Y.; Gao, Z.; Zhang, X. Integrated fault tolerant tracking control for rigid spacecraft using fractional order sliding mode technique. *J. Franklin I.* **2020**, *357*, 10557–10583. [CrossRef]
27. Fang, Y.; Li, S.; Fei, J. Adaptive Intelligent High-Order Sliding Mode Fractional Order Control for Harmonic Suppression. *Fractal Fract.* **2022**, *6*, 482. [CrossRef]
28. Cao, S.; Sun, L.; Jiang, J.; Zuo, Z. Reinforcement learning-based fixed-time trajectory tracking control for uncertain robotic manipulators with input saturation. *IEEE T. Neur. Net. Lear.* **2021**, *34*, 4584–4595. [CrossRef] [PubMed]
29. Chen, R.Z.; Li, Y.X.; Ahn, C.K. Reinforcement-learning-based fixed-time attitude consensus control for multiple spacecraft systems with model uncertainties. *Aerosp. Sci. Technol.* **2023**, *132*, 108060. [CrossRef]
30. Wang, X.; Shi, P.; Wen, C.; Zhao, Y. Design of parameter-self-tuning controller based on reinforcement learning for tracking noncooperative targets in space. *IEEE T. Aero. Elec. Sys.* **2020**, *56*, 4192–4208. [CrossRef]
31. Muduli, R.; Jena, D.; Moger, T. Application of Reinforcement Learning-Based Adaptive PID Controller for Automatic Generation Control of Multi-Area Power System. *IEEE T. Autom. Sci. Eng.* **2024**, 1–12. [CrossRef]
32. Nohooji, H.R.; Zaraki, A.; Voos, H. Actor–critic learning based PID control for robotic manipulators. *Appl. Soft Comput.* **2024**, *151*, 111153. [CrossRef]

33. Ouyang, Y.; Dong, L.; Wei, Y.; Sun, C. Neural network-based tracking control for an elastic joint robot with input constraint via actor-critic design. *Neurocomputing* **2020**, *409*, 286–295. [CrossRef]
34. Patel, B.M.; Dwivedy, S.K. Manoeuvring of underwater snake robot with tail thrust using the actor-critic neural network super-twisting sliding mode control in the uncertain environment and disturbances. *Neural. Comput. Appl.* **2023**, 1–15. [CrossRef]
35. Wang, N.; Gao, Y.; Zhao, H.; Ahn, C.K. Reinforcement learning-based optimal tracking control of an unknown unmanned surface vehicle. *IEEE T. Neur. Net. Lear.* **2020**, *32*, 3034–3045. [CrossRef] [PubMed]
36. Zheng, M.; Wu, Y.; Li, C. Reinforcement learning strategy for spacecraft attitude hyperagile tracking control with uncertainties. *Aerosp. Sci. Technol.* **2021**, *119*, 107126. [CrossRef]
37. Cao, J.; Zhang, Y.; Ju, C.; Xue, X.; Zhang, J. A New Force Control Method by Combining Traditional PID Control with Radial Basis Function Neural Network for a Spacecraft Low-Gravity Simulation System. *Aerospace* **2023**, *10*, 520. [CrossRef]
38. Yu, B.; Du, H.; Ding, L.; Wu, D.; Li, H. Neural network-based robust finite-time attitude stabilization for rigid spacecraft under angular velocity constraint. *Neural. Comput. Appl.* **2022**, *34*, 5107–5117. [CrossRef]
39. Jing, C.; Du, H.; Liu, Y.; Yan, B.; Liu, C. Immersion and invariance sliding mode control with time-delay estimation for rigid spacecraft with uncertainties and actuator faults. *T. I. Meas. Control* **2023**, *45*, 3138–3146. [CrossRef]
40. Muñoz-Vázquez, A.J.; Sánchez-Torres, J.D.; Parra-Vega, V.; Sánchez-Orta, A.; Martínez-Reyes, F. A fractional super-twisting control of electrically driven mechanical systems. *T. I. Meas. Control* **2020**, *42*, 485–492. [CrossRef]

Disclaimer/Publisher's Note: The statements, opinions and data contained in all publications are solely those of the individual author(s) and contributor(s) and not of MDPI and/or the editor(s). MDPI and/or the editor(s) disclaim responsibility for any injury to people or property resulting from any ideas, methods, instructions or products referred to in the content.